Anisotropic roughening of vicinally miscut Ag(110): X-ray-reflection profile analysis using the domain-matrix method

S. Pflanz, H. L. Meyerheim, and W. Moritz
Institut für Kristallographie und Mineralogie der Universität, Theresienstrasse 41, D-80333 München, Germany

I. K. Robinson
University of Illinois at Urbana-Champaign, Urbana, Illinois 61801

H. Hoernis and E. H. Conrad
School of Physics, Georgia Institute of Technology, Atlanta, Georgia 30332
(Received 20 May 1994; revised manuscript received 14 February 1995)

The roughening behavior of a vicinally miscut Ag(110) surface has been studied with x-ray diffraction using synchrotron radiation. The lateral profiles recorded at different $q_\perp$ were analyzed with (a) the domain-matrix method, an evaluation scheme for diffraction profiles, and (b) using a conventional power-law profile shape analysis. Both methods result in a roughening temperature of $T_R = 900 \pm 20$ K ($= 0.73 T_m$). The type of the roughening transition is consistent with the predictions of the anisotropic body-centered solid-on-solid (=six-vertex) model with step creation energies of $J_x = 45 \pm 3$ meV and $J_y = 60 \pm 3$ meV along $[\bar{1}10]$ and [001], respectively. At low temperatures, a two-component (bimodal) step distribution corresponding to a bunching of steps is identified.

I. INTRODUCTION

The idea of a surface roughening transition[1] as originally developed by Burton and Cabrera in 1949 (Ref. 2) has been confirmed by a number of experimental studies on meal surfaces.[3–15] While a number of studies dealt with open faces, such as, e.g., fcc(711), fcc(511), and fcc(311) (Refs. 3–8) (where roughening occurs at the step edges), the more recent work[9–15] focused on close-packed surfaces where adatom-vacancy pairs are generated on a surface that, at low temperatures, is free of steps.

The roughening principle, namely the existence of a high-temperature rough phase for purely entropic reasons, is usually discussed for surfaces perfectly aligned to a low-index crystallographic plane. The low-temperature nature of vicinally miscut surfaces at present is controversial, however. Discrepancies have been reported between experimental and theoretical diffraction line shapes on slightly miscut Ni,[10] Ag,[14,15] and Cu (Ref. 16) (110) surfaces in the low-temperature phase below T_R. Asymmetrical line shapes or line shapes consisting of a superposition of two or more unresolved peaks, inconsistent with the theoretical one-component line shapes,[1] have been reported,[10,14,15,16] and by some authors attributed to a faceting of the surface. Questions have been raised about the general applicability of the standard (Kosterlitz-Thouless) roughening theory[1] for such misaligned surfaces.[14]

In this paper, we focus on this problem and investigate the step distribution and its temperature dependence at the slightly misaligned Ag(110) surface. This surface has been investigated previously where the occurrence of shoulders in the beam profile and their characteristic shift with the momentum transfer normal to the surface have been attributed to faceting. This had been explained in a macroscopic picture with the cusp in the surface energy in the Wulff construction.[14] A later scanning-tunneling-microscopy (STM) study saw facets due to step bunching which were considered to be due to impurities pinning the steps.[17,18] The purpose of this paper is the determination of the step distribution and its change with temperature from a detailed analysis of the beam profiles. While we cannot identify the origin of the step distribution, we show that a two-component (bimodal) terrace width distribution produces the observed asymmetrical diffraction profiles. We apply a profile calculation approach (the domain-matrix method,[19] denoted DMM in the following). The temperature dependence of the terrace width (step-step distance) distribution has been studied in two lattice directions, along $[\bar{1}10]$ and [001], and the result shows that near the roughening temperature the distribution approaches a geometric distribution similar to the roughening of a flat surface. In addition to the direct determination of step distribution functions with the DMM, we have analyzed the profiles at the out-of-phase diffraction condition with the conventional method assuming a power-law profile with an exponent η. The solid-on-solid (SOS) theory of roughening is, strictly speaking, not valid for a vicinal surface which exhibits step bunching or faceting. We include this analysis, however, for comparison with previous studies. With both methods a roughening transition temperature of $T_R = 900 \pm 20$ K (corresponding to $0.73 T_m$) is obtained. Ignoring the slight miscut at higher temperatures, we have further determined the step energies J_x and J_y along $x = [\bar{1}10]$ and $y = [001]$ using the anisotropic BCSOS model (body-centered solid-on-solid model[20]) appropriate for fcc(110) surfaces.

0163-1829/95/52(4)/2914(13)/$06.00

The DMM has the additional advantage that a general form of terrace width (step-step distance) distribution function (and not only its height-height correlation function) can be handled appropriately. This allows an exact description of rough surfaces (along both azimuths), even those containing a considerable amount of miscut.

The paper is organized as follows: Sec. II gives a short description of the experiments. In Sec. II A we describe the domain-matrix method and its applications. In Sec. III the roughening behavior is studied using the DMM (Sec. III A) and the power-law analysis (Sec. III B), and the step energies are determined (Sec. III C). The results obtained by the different data analysis methods are summarized in Sec. IV.

II. EXPERIMENT

The measurements were performed at the beamline X16A of the National Synchrotron Light Source (NSLS) storage ring at the Brookhaven National Laboratory using the four-circle diffractometer operated in the five-circle mode.[21] Prior to mounting the crystal into the UHV chamber the surface was oriented, polished, and chemically etched using a 50% HNO_3 solution. Final cleaning was achieved under UHV conditions by long-term (several hours) Ar^+-ion sputtering (500 eV) and subsequent annealing at 800–1000 K by radiative heating using a filament. All measurements were carried out at an x-ray energy of 11.6 keV, and the lattice parameter was effectively corrected for thermal expansion. The sample was aligned using bulk Bragg reflections (301) and (031) (in the surface-adapted orthorhombic setting[22]). Slits of 2 mm (in-plane) and 10 mm (out-of-plane) mounted 600 mm in front of the NaI scintillation detector provided an in-plane longitudinal resolution of $\Delta q_{\parallel}=1.9\times10^{-2}$-Å^{-1} full width at half maximum (FWHM) and a perpendicular resolution of $\Delta q_{\perp}=9.8\times10^{-2}$-Å^{-1} FWHM, the latter corresponding to about 0.05 reciprocal-lattice units.[22] All data shown here are transverse scans (ω scans) whose resolution is only limited by the sample mosaic which can well be described by a Gaussian of $\approx$0.002 reciprocal-lattice units FWHM.[22] Care was taken during the sample annealing and cooling cycles in order to reach equilibrium conditions. Each scan was taken after several minutes of waiting at a given temperature. The accuracy of the temperature setting (using a Pt resistance) is estimated to be better than ±3 K.

The recorded data sets consist of lateral diffraction profiles [the ($\bar{1}0l$) and the ($01l$) rods in the surface-adapted orthorhombic setting[22]] recorded along the (cubic) directions $q_{\parallel}=[\bar{1}10]$ and [001] at different $q_{\perp}$. In the following, we use $q_{\parallel}a=2\pi h$, $q_{\parallel}b=2\pi k$, and $q_{\perp}c=2\pi l$, and take the reciprocal coordinates (hkl) in the orthorhombic setting whereby h corresponds to [001] and k to [$\bar{1}$10]. The in-plane lattice constants are $a=4.086$ Å and $b=2.889$ Å, and the layer spacing is $d_{\perp}=2.889$ Å$/2=1.44$ Å. The experimental profiles of the ($\bar{1}01$) and (011) rods measured along [$\bar{1}$10] and [001] (transverse scans) are shown in Fig. 1 at $l=0.1$, 0.5, and 0.7. Note that for these rods the in-phase condition (where the terraces separated by a step scatter in phase) is at $l=1$, whereas the out-of-phase condition (where the terraces scatter out of phase) occurs at $l=0$.

A. The domain-matrix method and different step models

For a calculation of the diffraction profiles from arbitrary step distributions we used, as already mentioned, the domain-matrix method.[19] This calculation scheme is based on the assumption of one-dimensional disorder. The reflected intensity is calculated from a transition matrix $p_{\alpha\beta}$ which contains the probabilities to find a domain of type β next to a domain of type α. The quantities $p_{\alpha\beta}^{(l)}$ (the lth powers of p) then describe the probability to find a domain of type α in a distance of l domains from one of type β. Together with the *a priori* probabilities p_{α} (the probabilities to find a domain of type α anywhere on the surface) it therefore holds that

$$p_{\alpha,\alpha'}^{(l)}=\sum_{\beta}p_{\alpha\beta}^{(l-1)}p_{\beta\alpha'}\ ,\quad p_{\alpha}=\lim_{l\to\infty}p_{\alpha\alpha'}^{(l)}\ , \tag{1}$$

where for large distances the correlations vanish. The number of domain types now depends on the problem,

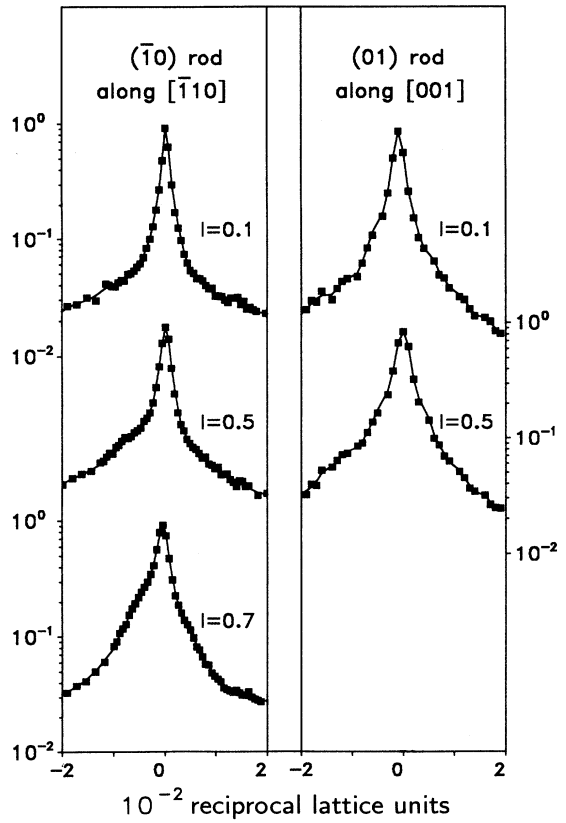

FIG. 1. Experimental profiles recorded at 300 K on the Ag(110) surface along [$\bar{1}$10] [the ($\bar{1}$0) rod] and [001] [the (01) rod] at different l. The in-phase condition is at $l=1$, the out-of-phase condition at $l=0$. Note that the profiles show a second component that is strongly visible along [$\bar{1}$10], but almost not along [001]. At $l=0.1$ the profiles along [001] are clearly broader, indicating that the main step direction is along [$\bar{1}$10].

and can be chosen appropriately. A facet model with two facets, for instance, is well described by two domain types (the two-facet orientations), while a rough surface requires three domain types: upward steps, downward steps, and terraces (no steps). We consider a step as a separate domain and in the corresponding width distribution only one value occurs (namely one) when only single steps are considered. The description with three domain types has the advantage that the occurrence of multiple steps (usually present on rough surfaces) can be included. It should be noted that the lattice vector can be chosen separately for each domain type in the DMM.

Each domain is described by a structure factor $F_\alpha^{w_\alpha}$ that depends on the width w_α of the domain of type α. For a homogeneous chain, the diffracted intensity of the domain structure can then be computed by averaging over all possible arrangements of domain types (and their respective sizes along the chain), which finally gives

$$I(\underline{q})=\sum_l \sum_{\alpha\alpha'} p_\alpha p_{\alpha\alpha'}^{(l)} \sum_{w_\alpha w_{\alpha'}} v_\alpha(w_\alpha) v_{\alpha'}(w_{\alpha'}) [F_\alpha^{w_\alpha} F_{\alpha'}^{*w_{\alpha'}}] \times \Phi(\alpha,\alpha',w_\alpha,w_{\alpha'},l) \ . \quad (2)$$

Thereby the quantities $v_\alpha(w)$ describe the width distribution of the domains of type α. The interdomain phase factor $\phi(\alpha,\alpha',w_\alpha,w_{\alpha'},l)$ takes account of the geometrical phase difference between the domain pair (α,α') which is separated by $l-1$ intervening domains. The calculation of this phase factor is the central point of the problem. Unlike the matrix method applied to a sequence of unit cells an analytic expression cannot be given and the calculation is done iteratively, again averaging over all possible domain types (and lengths) between the first and lth domains along the chain (see also Ref. 19).

The coverage θ_α, finally, fixing the amount to which the respective domain types occur on the surfaces, are determined by p_α weighted with the average width $\langle w_\alpha \rangle$ of the domains of type α; thus

$$\Theta_\alpha=\frac{p_\alpha \langle w_\alpha \rangle}{\sum_\alpha p_\alpha \langle w_\alpha \rangle} \ , \quad \langle w_\alpha \rangle = \sum_w v_\alpha(w) w \ . \quad (3)$$

The explicit form of the transition matrix p for the models studied now in more detail [and fitted via Eq. (2) to the diffraction profiles] are discussed in more detail in Sec. II B.

B. DMM analysis of the low-temperature state

With the DMM we have now calculated possible step arrangements of the vicinally miscut Ag(110) surface. Four models have been considered which, together with the corresponding step-step distance distributions, are shown in Fig. 2. In Fig. 2(a) a two-facet structure is shown; in Fig. 2(b) a surface with a single-component step distribution, i.e, a distribution with a single maximum; in Fig. 2(c) one with a two-component step distribution; and in Fig. 2(d) a structure consisting of rougher tilted and flatter untilted surface parts. The last structure, a so-called *hill-and-valley* structure,[23] corresponds to faceting where large flat terraces exist and facets with a certain range of facet angles. The difference in model (c) is that facets close to the [110] orientation are excluded. Model (d) had been previously proposed for the misaligned Ag(110) surface.[14] In Fig. 2(c) a two-dimensional step distribution is drawn to illustrate that a correlation between the step distributions in both lattice directions should exist when a crossing of steps is excluded. This may be considered as a possible cause for the observed bimodal step distribution.

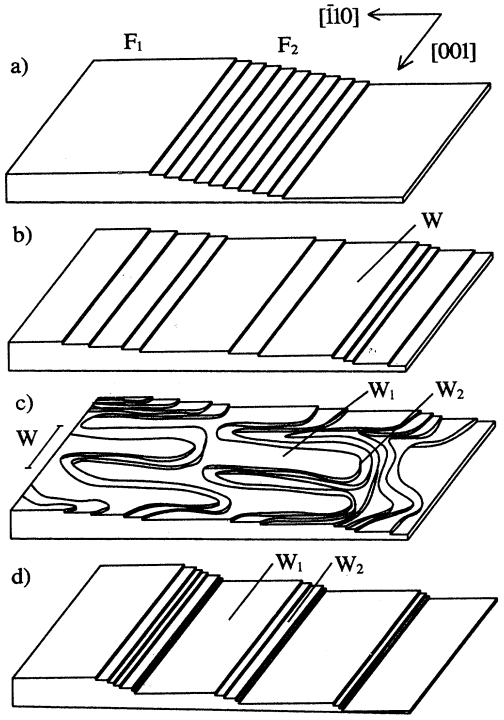

FIG. 2. The four models tested for the low-temperature state of the Ag(110) surface: (a) the facet model, (b) the single-component step model, (c) the two-component (bimodal) step model with meandering steps, and (d) a hill-and-valley structure.

Let us first focus on the question whether facets [Fig. 2(a)] or a step distribution function with a single maximum [Fig. 2(b)] could explain the observed diffraction profiles. Both models represent extreme cases of a vicinally miscut surface. The facet model, consisting of two smooth facets, is described by $p_1=p_2=0.5$ and the correlation matrix

$$P=\begin{bmatrix} 0 & 1 \\ 1 & 0 \end{bmatrix} , \quad (4)$$

which means that domain 1 follows domain 2 and vice versa. Note that structure factors describing atoms within the unit cells of both facets depend on the facet orientation. To respect the macroscopic miscut angle α_0 a *lever rule* must hold:

$$\frac{\sum_i \langle w_i \rangle \sin(\alpha_i)}{\sum_i \langle w_i \rangle \cos(\alpha_i)} = \tan(\alpha_0) , \tag{5}$$

whereby α_1, α_2 and $\langle w_1 \rangle, \langle w_2 \rangle$ are the orientation angles and average widths (in Å) of the two facets. The widths of the facets (in units of the facet unit cell) are described by $v_1(w)$ and $v_2(w)$ in Eq. (2) can be varied according to different width distribution functions. For large facets, however, it turns out that details of $v_1(w)$ and $v_2(w)$ are irrelevant for the diffraction profile, because then the incoherent sum of both contributions is visible in the profile. Consequently, two reciprocal-lattice rods arise. In the calculated example, the first one is tilted and the second one is not. Figure 3(a) shows the corresponding reflection profiles whereby broad distribution functions $v_1(w)$ and $v_2(w)$ of Gaussian type and $\langle w_1 \rangle = 3750$ Å and $\langle w_2 \rangle = 2900$ Å (widths along $[\bar{1}10]$) have been assumed; the corresponding tilt angle is then [Eq. (5)] 0.125°. Figure 3(a) shows that the result is a sharp satellite which moves with $l(2\pi l = q_\perp c)$ in its lateral position. The comparison with the experimental profiles [Fig. 3(c), points] shows clearly that a two-facet structure as shown in Fig. 2(a) is not present on the misaligned Ag(110) sample at 300 K. Smaller facets and other size distributions would not change this picture unless the facets become so small that a description with a step distribution is more appropriate.

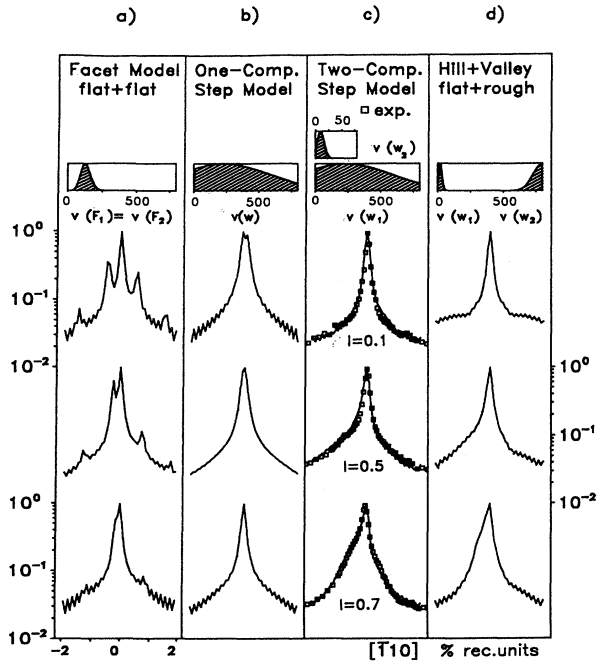

FIG. 3. Calculated profile shapes along $[\bar{1}10]$ at $l = 0.7$, 0.5, and 0.1 for (a) the facet model, (b) the single-component step model (c) the two-component step model, and (d) the hill-and-valley structure in comparison with the experimental profiles (squares) at 300 K. The calculated profiles were convolved with a Gaussian of 0.002 reciprocal lattice units FWHM to respect instrumental resolution. In the upper panel the distribution functions $v(w)$ are visualized.

The next model is the one-component step model [Fig. 2(b)]. In this model the distribution of the step distances is an analytical function such as, e.g., a Gaussian or an exponential (geometrical) size distribution function. For the calculation with the DMM method we assume the flat terrace as a domain of type 1, the upward steps as type 2, and the downward steps as type 3. We assume that only single steps exist. The correlation matrix is

$$P = \begin{bmatrix} 0 & \frac{r}{r+1} & \frac{1}{r+1} \\ 1 & 0 & 0 \\ 1 & 0 & 0 \end{bmatrix} . \tag{6}$$

The parameter r describing the ratio between up and down steps takes the surface asymmetry into account. As for the facet model, a lever rule holds:

$$\frac{a\langle w \rangle}{d_\perp} = \frac{1-r}{1+r}(\tan\alpha_0)^{-1} , \tag{7}$$

whereby $\langle w \rangle$ is the average terrace width and a the lattice constant. A typical result for the one-component step model is shown in Fig. 3(b), whereby, as in the facet model, a broad truncated Gaussian function has been assumed for $v(w)$. The profile now splits into two diffraction peaks at $l = 0.1$ (with l the vertical scattering phase). This effect, appearing close to the out-of-phase condition $l = 0$ for the (10) rod (where both components become equally strong), is a well-known fact for steps with a preferred size distribution that generates an *average superlattice.* As this splitting is absent in the experimental profiles [Fig. 3(c), points] and, on the other hand, occurs for every distribution function we tested (such as Gaussian, Poisson, and algebraic distributions, not shown here), we are led to the conclusion that neither model (b) nor model (a) is the correct model for the vicinally miscut Ag(110) surface. Having ruled out models (a) and (b), we tested models (c) (two-component step model) and (d) (hill-and-valley structure) assuming Gaussian functions for both components of the distribution function.

We first focus on the two-component or bimodal step model with meandering steps as depicted in Fig. 2(c). This model possesses a step distribution with two maxima and therefore consists of parts of broader terrace widths in coexistence with parts of smaller terrace widths. The main step direction in this model, however, does not fall into the misaligned azimuth, but is perpendicular to it. This means that the origin of this special step arrangement is not the misalignment alone, but also the anisotropy of the surface that makes steps along $[\bar{1}10]$ at a lower cost available than along [001].

To now describe the two size distributions of the flat terraces in model (c), four domain types are necessary. These are the broader terraces (type 1), the upward steps (type 2), the smaller terraces (type 3), and the downward steps (type 4). Using this order, for a correlation matrix along $[\bar{1}10]$ and along [001] we obtain

$$P_{[\bar{1}10]}=\begin{bmatrix} 0 & \frac{r_1}{r_1+1} & 0 & \frac{1}{r_1+1} \\ 1-s & 0 & s & 0 \\ 0 & \frac{r_2}{r_2+1} & 0 & \frac{1}{r_2+1} \\ 1-s & 0 & s & 0 \end{bmatrix}, \qquad P_{[001]}=\begin{bmatrix} 0 & \frac{1}{2} & \frac{1}{2} \\ 1 & 0 & 0 \\ 1 & 0 & 0 \end{bmatrix}. \tag{8}$$

Each step is followed by either a smaller terrace described by $v_2(w)$ (probability: s) or a broader terrace described by $v_1(w)$ (probability: $1-s$). Consequently, we obtain two misorientation parameters r_1 and r_2 which are now the ratio of upward to downward steps for components one and two. The parameter s fixes the area of the rough phase θ_2 (in unit cells). Noting the area of the smoother phase by θ_1, we further obtain

$$\theta_1=\frac{(1-s)\langle w_1\rangle}{(1-s)\langle w_1\rangle+s\langle w_2\rangle}, \qquad \theta_2=\frac{s\langle w_2\rangle}{(1-s)\langle w_1\rangle+s\langle w_2\rangle}. \tag{9}$$

Along [001] we do not distinguish between broader and smaller terraces, and therefore can use a (3×3) correlation matrix. This handling is justified because the experimental profiles along [001] (Fig. 1) exhibit neither a pronounced shoulder nor a pronounced asymmetry in the [001] azimuth. The parameter s measures the amount of step bunching along $[\bar{1}10]$; $s=0$ corresponds to absence of bunching. A fit of s to the experimental diffraction profiles (Fig. 3, points) now shows that s is nonvanishing below T_R. A step bunching with rough (meandering) steps is therefore present at room temperature. The parameters r_1 and r_2 as well could be determined from fits to the profiles. The sensitivity to the parameter r_1, however, is very small because it essentially shifts slightly only the central peak in the profile (about ≈0.001 reciprocal lattice units). We therefore fitted only r_2. In the following we denote this value as r. Figure 3(c) shows the best-fit results obtained for model (c) in comparison with the experimental profile [points in Fig. 3(c)]. It is obvious that model (c) gives a much better agreement than the previously discussed models. Before discussing this in more detail, we describe model (d), the *hill-and-valley* structure, with an exclusion of certain terrace sizes corresponding to a phase separation.

To describe model (d) we can use the identical transition matrix as in model (c) [Eq. (8)], but with the difference that $v_1(w)$ and $v_2(w)$ now represent step distances in the flatter (untilted) and rougher (tilted) surface areas. Physically, the hill-and-valley structure is stabilized by a cusp in the equilibrium crystal shape (EQS theory[23,24]) which, in the mean-field approach and at low temperatures, should lead to a gap in the surface orientations along $[\bar{1}10]$. Strictly speaking, this is only correct in the mean-field approach and at $T=0$ K, but we can assume that 300 K is still a low temperature. We therefore have chosen $v_1(w)$ and $v_2(w)$ in such a way that they do not overlap significantly (Fig. 3, upper inset).

From Fig. 3(d) it is obvious that model (d) describes the profile data along $[\bar{1}10]$ almost equally well as model (c). Both models differ only slightly and the details of the distribution function obviously cannot be extracted from the diffraction profiles. It follows that both models (c) and (d) are appropriate descriptions of the low-temperature state along $[\bar{1}10]$, making both the hill-and-valley structure and the meandering step model possible. There is, however, a relevant difference in the profile shapes along [001] for the two models (c) and (d). While model (c) is consistent with broader profiles along [001] than along $[\bar{1}10]$, this is less likely for model (d) because the existence of all terrace sizes along [001] makes the assumption of a gap in $[\bar{1}10]$ unrealistic. From the anisotropy of the profile shapes along both azimuths it thus follows that model (c) and not model (d) is the most reasonable approach to the low-temperature state of the misaligned Ag(110) surface studied here.

We finally note that, for models (c) and (d), Gaussian distributions of fitable widths have been assumed for $v(w_1)$ and $v(w_2)$. Details of these distribution types, however, turned out to be not very significant. The important point, however, is that for both models broad shoulders occur in the diffraction profiles that decrease in intensity from the in-phase condition $l=1$ to the out-of-phase condition $l=0$, exactly as in the experimental profiles. This clearly shows that models (c) or (d) and not (a) or (b) are correct.

In summary, from the profile analysis it follows that the Ag(110) surface, misaligned by 0.1°–0.2° along $[\bar{1}10]$, exhibits a bunching of steps at low temperatures. This result is confirmed by recent STM studies on vicinally miscut Ag(110) surfaces.[17,18] In Ref. 17 the bunching has been attributed to defects (e.g., dislocation lines or residual oxygen) that pin and locally bend the steps. By Auger electron spectroscopy (AES) we could not detect any defects within our resolution limit of $\approx1\%$ of a monolayer. According to Ref. 18, however, even densities lower than 0.1% (far below our AES detection limit) can produce step bunching. A defect-induced step bunching is thus a possible scenario for our (and also the previously studied) misaligned sample(s). Another explanation, not using defects, is also worth considering: A crossing of straight steps is energetically unfavorable and leads to an interconnection between terraces and curved steps. The exclusion of step crossing may then act as a repulsive potential for all pairs of steps that meander oppositely (out of phase), but as an effective attractive potential for steps that meander uniformly (in phase). Such simple energetic arguments could possibly explain the identified bimodal step distribution at low temperatures. Further theoretical calculations [such as, e.g., the calculations of den Nijs and co-workers[25] for models with competing nearest-neighbor (NN) and next-nearest-neighbor (NNN) interactions] including both the miscut and surface anisotropies (and, possibly, the additional potential of defects) are thus necessary to elucidate the

reason for the step bunching in more detail.

The best-fit parameters obtained by fitting model (c) to the experimental data (300 K) are $\langle w_1 \rangle = 230$, $\langle w_2 \rangle = 10$, $r = r_2 = 0.15$, and $s = 0.9$. The last value means a relative good separation of areas with bunched steps and flat terraces. From the fit values obtained, miscut angles α_1 and α_2 of the smoother and rougher surface areas along $[\bar{1}10]$ can be derived. In a previous study[14] resulting in quite similar (multicomponent) diffraction profiles the macroscopic miscut angle α_0 of the sample was measured to be $\approx 0.19°$ along $[\bar{1}10]$ and $\approx 0.10°$ along [001], while $\alpha_0 = 0.14°$ was determined from the fitting of two Lorentzians to the profiles along $[\bar{1}10]$. As here we used the same sample and the same diffractometer setting, we expect a similar miscut of $0.1°$–$0.2°$. Using the average orientation $\alpha_0 = 0.14 \pm 0.05°$ (the value of Ref. 14) and

$$(\tan\alpha_0)^{-1} = \left[\frac{1+r_1}{1-r_1}(1-s)\langle w_1 \rangle + \frac{1+r_2}{1-r_2} s \langle w_2 \rangle \right] \frac{a}{d_\perp} , \tag{10}$$

for the misorientation parameter of the first component we obtain a relatively high value of $r_1 = 0.78$. This value means that the symmetry of the flatter surface parts ($r_1 = 0.78$) exceeds that of the rougher surface parts ($r_2 = 0.25$), which again shows that some steps must be bunched.

We finally note that the domain width distribution functions $v(w)$, used in the DMM calculations and depicted in the insets of Fig. 3, are not the same quantities as the coverages of the surface with domains of width w. The latter are the products $wv(w)$. The relation between $v(w)$ and the coverage is visualized in Fig. 4 for some terrace size distribution functions.

III. ROUGHENING BEHAVIOR OF Ag(110) SURFACE

A. Analysis using domain-matrix method

1. $[\bar{1}10]$ azimuth

Along the $[\bar{1}10]$ azimuth we have now fitted the bimodal step model, discussed in Sec. II B, to the experimental profiles at temperatures between 300 and 900 K. Figure 5(a) shows some of these fits [using Eq. (8)] on a logarithmic scale. Transverse scans through the $(\bar{1}0l)$ rod (scans along $[\bar{1}10]$) at $l = 0.5$ between 300 and 770 K are shown as open circles, and the fits to this model as solid lines. The dashed lines in Fig. 5(a) indicate symmetric line shapes for comparison. The shaded regions mark the asymmetry of the reflection profiles arising mainly from the rough component in this model. The scans were performed along the $[\bar{1}10]$ azimuth, which is the direction of the close-packed rows in the (110) surface. The analysis was performed at $l = 0.5$, between in-phase and out-of-phase conditions, since here the step-induced asymmetry, arising from the different phase shifts of up and down steps, and therefore the sensitivity to the parameter $r = r_2$, are at its maximum.

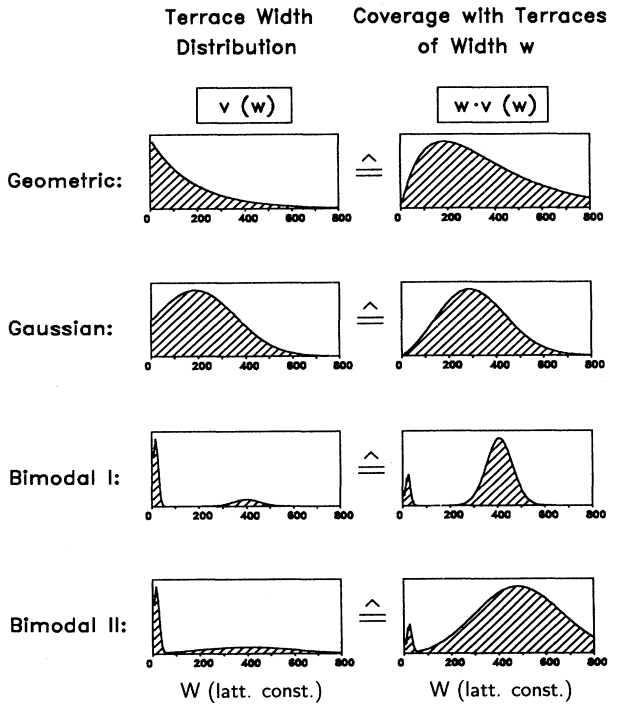

FIG. 4. Relation between the distribution function $v(w)$ and the coverage of the surface with terraces of width w, measured by $wv(w)$, for some step distribution functions.

The fit parameters [using Eq. (2) with the correlation matrix of Eq. (8)] were the maximum and the width of the two (truncated at zero) Gaussian distribution functions $v_1(w)$ and $v_2(w)$ and the parameters r (ratio between up and down steps) and s (phase separation or step bunching parameter; see Sec. II B). At $s = 0.5$ no distinction between areas with high and low step densities can be made, and the surface is then in a homogeneous state. Besides r, s, $v_1(w)$, and $v_2(w)$, we fitted the background (as a constant) and convoluted the reflection profile with a Gaussian resolution function of 0.002 FWHM rec. units. The upper inset of Fig. 5(a) shows the obtained step distribution functions for some of the profiles and the low inset how r and s change with temperature.

Let us first concentrate on the terrace width distribution of the smaller terraces $v_2(w)$ and the development of the parameter s. As Fig. 5(a) shows, $v_2(w)$ essentially remains constant for all temperatures while s decreases from 0.9 at 300 K at about 0.5 at T_R [lower inset of Fig. 5(a)]. The area of the bunched steps (given by θ_2) therefore decreases with temperature. This obviously means that the flat regions show a stronger roughening than the already rough regions, and that the surface thus becomes more homogeneously rough.

The roughening of the smoother surface areas is visible in the change of $v_1(w)$ with temperature. This distribution has been parametrized by the first two moments—the average length $\langle w \rangle$ and the half-width $\langle (w - \langle w \rangle)^2 \rangle^{1/2}$—assuming a Gaussian distribution. In this case $v_1(w)$ is completely determined. The decrease of the mean value $\langle w_1 \rangle$, plotted in the upper inset of Fig.

5(a), shows clearly that these areas roughen up. Though at all temperatures the half-width ($\langle(w-\langle w\rangle)^2\rangle^{1/2}$) of $v_1(w)$ remains large, additional steps are created on the surface, because the mean value of this distribution is shifted to much lower values as the temperature approaches T_R. At higher temperatures, the decreasing average terrace size $\langle w\rangle$ changes the character of the distribution function as well because $v_1(w)$ is truncated at $w=0$. The shifting of $\langle w\rangle$ must therefore change the correlation function as well, and this is obviously the reason for the observed profile shape changes.

To compare the (truncated) Gaussian distribution functions used for the fits with theoretical predictions, we first note that the roughening theory[1,20,26] does not directly predict the terrace width distribution, either for $T<T_R$ or for $T>T_R$. Instead a pair-correlation function is predicted which is related to the terrace width distribution by multiparticle theory,[27–29] and an application to miscut surfaces has not explicitly worked out so far.

The truncated Gaussian distribution that fits well to the central part (-0.015 to 0.015 rec. units) of the profiles measured along [$\bar{1}10$] [Fig. 5(a)] is, however, in at least qualitative agreement with the calculations of Kariotis,[27] Kariotis and Lagally,[28] and Bartelt, Einstein, and Williams,[29] who for vicinal surfaces at lower temperatures predicted a similar Gaussian-like distribution function. These theories,[27–29] that explicitly respect step-step interactions on a vicinal surface through a step-binding energy term, predict in the high-temperature limit a geometric terrace width distribution (purely *entropic* steps) with a crossover behavior in between. We did not try our fits to resolve the changes in the distribution functions, but chose the Gaussian distribution function which fitted well between -0.015 and 0.015 reciprocal lattice units at all investigated temperatures.

At 300 K, we tested a number of other distribution functions, for comparison with the Gaussian distribution type. Geometric, Poisson, rectangular, and algebraic distributions, however, did not lead to reasonable agreement at low temperatures (300 K) and were therefore considered as unprobable. The R_u factors (unweighted residuals) of some of these distributions are shown in Fig. 6.

There are some more results that can be derived from the fits shown in Fig. 5(a). The shift of the Gaussian distribution function to lower $\langle w_1\rangle$ with increasing temperature can be interpreted as the increased formation of

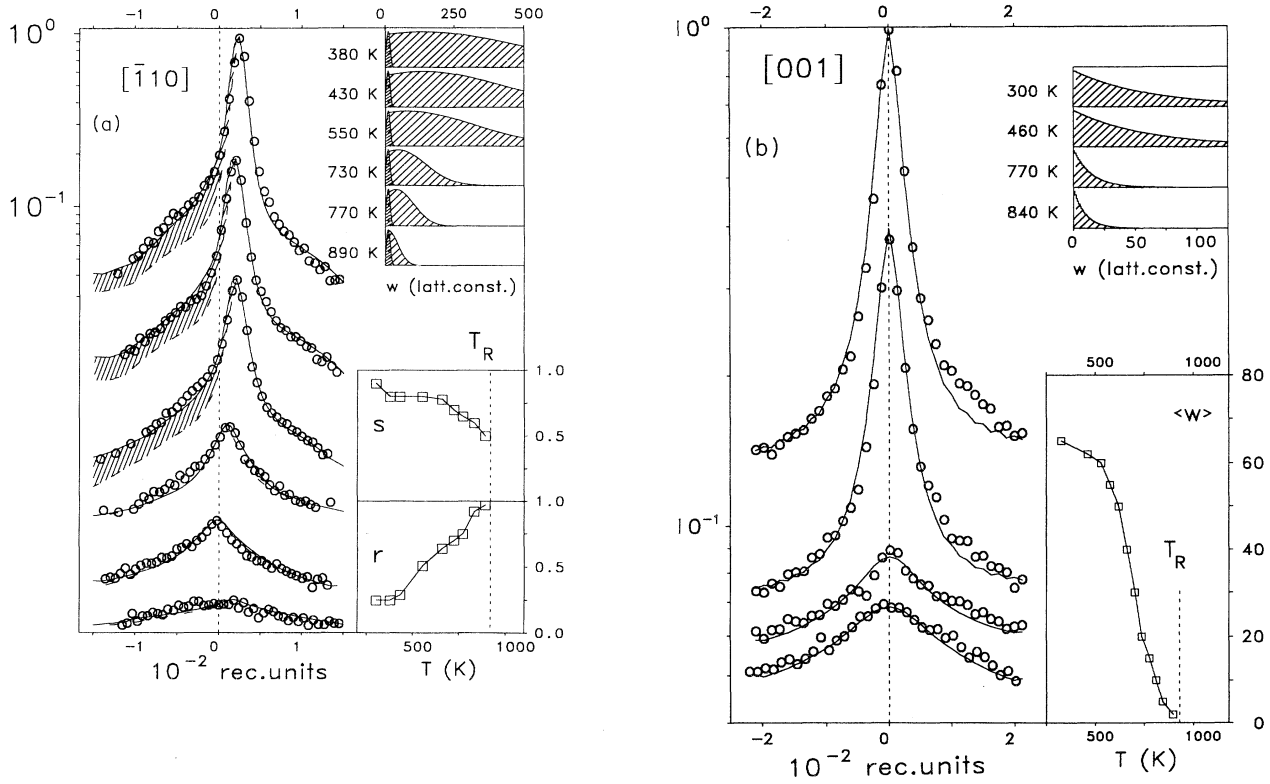

FIG. 5. (a) Fit of the experimental profiles along [$\bar{1}10$] at $l=0.5$ [transverse scan through the ($\bar{1}0$) rod] with the two-component step model (solid lines). Dashed lines indicate symmetric profiles for comparison, and the hatched region marks the profile asymmetry. The Gaussian terrace width distributions $v(w)$ used for the fits are shown in the upper inset, and the development of s and r is shown in the lower insets. Roughening is characterized by the asymptotic point $r=1$ at $\approx$900 K. (b) Fit of the experimental profiles along [001] at $l=0.5$ [transversal scan through the (01) rod] with the single-component step model (solid lines). The geometric terrace width distributions $v(w)$ used for the fits are shown in the upper inset, and the development of the average terrace width $\langle w\rangle$ is shown in the lower inset. The roughening is near $\langle w\rangle=2$, which indicates a high step density.

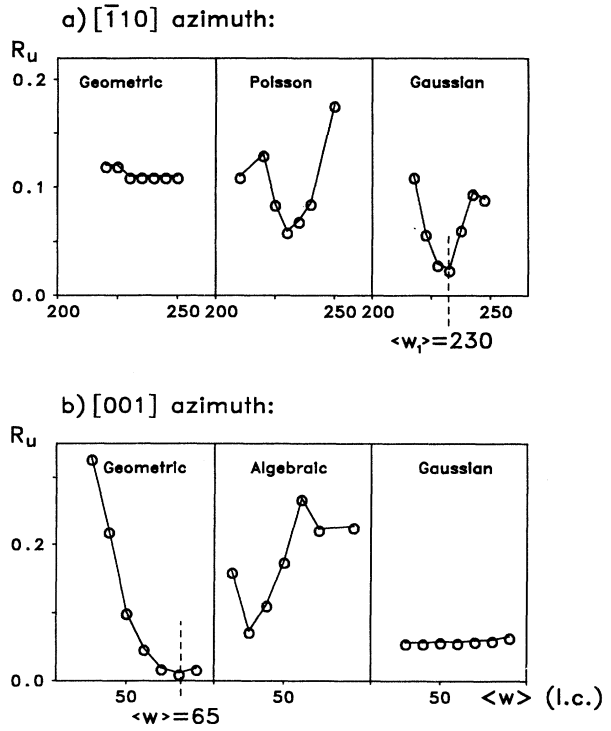

FIG. 6. Obtained R_u factors for different step-step distance distribution functions along both azimuths at 300 K. Along the [$\bar{1}$10] azimuth, the Gaussian distribution function with a broad fluctuation width $(\langle w^2\rangle\text{-}\langle w\rangle^2)^{1/2}$ gives the best agreement, while along [001] a geometric distribution function fits best.

multiatomic steps whose amount is proportional to $v_1(0)$. Simultaneously, we observe an increase of the step-up to step-down ratio $r=r_2$ which is shown in the lower inset of Fig. 5(a). The $r(T)$ behavior indicates the formation of an increasing number of up-steps on the surface that originally (along [$\bar{1}$10]) possessed mainly down-steps. The asymmetry of the surface is thus lifted with increasing temperature. This, of course, is only explainable by a roughening transition approach. Within this approach, the temperature at which $r(T)=1$ can be identified with the roughening temperature T_R. Thus $r=1$ taking as the roughening point, an extrapolation of the experimentally derived $r(T)$ behavior gives a roughening temperature of $T_R=900\pm50$ K [dashed line in Fig. 5(a), lower inset]. This temperature corresponds to the vanishing of the phase separation at $s=0.5$, which proves that the surface is *homogeneously* rough at T_R.

The obtained T_R value ($T_R=0.73T_m$) fits well into the series of the other fcc(110) surfaces that exhibit roughening temperatures of $0.69T_m-0.75T_m$ (for details, see Ref. 1). Finally, we note that our analysis of the [$\bar{1}$10] profiles [Fig. 5(a)] shows that at low temperatures (300 K) the Ag(110) surface with 0.14° misorientation exhibits a broad fluctuation width of $(\langle w^2\rangle\text{-}\langle w\rangle^2)^{1/2}\approx300$ lattice constants. In this phase, the step positions along both azimuths are widely disordered. Especially the miscut-induced steps (step edges along [001]) are curved and (on average) meandering, which explains the less-pronounced inhomogeneity identified along [001] (Fig. 1).

2. *[001] azimuth*

Along the [001] azimuth we have performed a step model analysis as along [$\bar{1}$10], but now using a single-component step distribution because a pronounced inhomogeneity is obviously not present along this azimuth. Figure 5(b) shows corresponding profiles of the (01) rod (scans along [001]) at $l=0.5$ and the fit to the random step model at different temperatures. The solid lines represent the fits to the random step model, assuming a geometric (exponential) terrace width distribution. For all fits we obtained unweighted residuals R_u lower than 5%, in most cases even below 2%.

First of all, there are clearly more steps visible along this azimuth, and the profile asymmetry is almost vanishing [Fig. 5(b)]. The best fit obtained for the random step model gives a mean step-step distance of 65 lattice units (260 Å), compared with the value of 230 lattice constants along [$\bar{1}$10] (680 Å), and thus a low-temperature surface step density asymmetry of about 3.5:1 at 300 K.

The miscut along the [001] azimuth is small ($\alpha_0<0.1°$), therefore no significant asymmetry can be observed and up- and down-steps are present with (almost) the same probability. In this case the terrace width distribution function is the only fit parameter. Different distribution functions have been tested as well as in the [$\bar{1}$10] azimuth for the profiles along [001]. Gaussian, Poisson, rectangular, and algebraic distributions, however, did not lead to a reasonable agreement in this azimuth at 300 K (see Fig. 6), and therefore were rejected.

Again the influence of different distribution functions has to be discussed from a theoretical point of view. First it is not astonishing that we do not find a Gaussian distribution (as in the misaligned azimuth), but a geometric function. If no miscut is presented, the ground state of the surface is without any steps. In this case, vicinal surface theories[27–29] are not applicable, but the conventional roughening theory[20,26] should hold. This theory predicts an algebraic-exponential pair-correlation function

$$P(r)=r^{-\eta}e^{-r/\xi} \tag{11}$$

that for $T<T_r$ (finite ξ and low η) is exponentially decaying at the high terrace widths. This is consistent with our finding of a best fit with a geometric terrace width distribution function which also describes an exponentially decaying $P(r)$. At T_R, ξ diverges and the pair correlation becomes algebraic. The algebraic $P(r)$ should also affect the terrace width distribution function, but an explicit form of $v(w)$ at T_R is not known to the authors (it is not directly the pair-correlation function[29]). We therefore did not try in our fits to resolve the subtle differences in the correlation function predicted by the roughening theory in this analysis, but instead chose the geometric distribution function which fitted well between -0.02 and 0.02 reciprocal lattice units at all temperatures and is in leading order consistent with the roughening theory (for $T<T_R$).

The thermal development of the mean terrace widths $\langle w\rangle$ obtained with the geometric distribution function is shown in the upper inset of Fig. 5(b). The extrapolation of the average terrace width $\langle w\rangle$ to $\langle w\rangle=2$, the

roughening point of the BCSOS model (Sec. III B), now provides another determination of the roughening temperature. We thus obtain $T_R = 900 \pm 50$ K [Fig. 5(b), lower inset] where the error has been estimated and essentially comes from the uncertainty of the exact terrace width distribution function that changes close to T_R. The obtained T_R value is consistent with the roughening point determined for the $[\bar{1}10]$ azimuth (≈ 900 K as well).

The difference in the step densities along $[\bar{1}10]$ and [001] at low temperatures must now be discussed. Obviously, it is *not at all* the miscut that is responsible for the different profile widths along both azimuths. The aligned [001] azimuth has a *higher* step density than the misaligned $[\bar{1}10]$ azimuth. We certainly can conclude that this is because of the difference in the step energy. Steps along [001] are less closely packed, form (100) microfacets, and are therefore energetically unfavored compared to the close-packed steps along $[\bar{1}10]$ that form (111) microfacets.

A theoretical model that describes this trend is the anisotropic BCSOS model[20,26] as well as the RSOS (restricted solid-on-solid) model of Rommelse and den Nijs[25] that predicts a DOF (disordered flat) phase in between flat and rough. In both models, the anisotropy of the step energies is explicitly taken into account and an anisotropic roughening transition is predicted. In Sec. III B, where we analyze the roughening exponent η, we will return to a discussion of these models.

B. Analyses of roughening exponent η

So far we have analyzed the roughening using an explicit step model solved by a numerical calculation scheme. An anisotropic step roughening transition was identified as an appropriate description for our Ag(110) sample. While this is not the traditional approach to model roughening, the use of an explicit step distribution model was necessary to include the miscut and the meandering and bunching of steps at low temperatures on our sample. The traditional approach used in other studies[1–14] is an analytical profile description using the Kosterlitz-Thouless roughening theory,[20,26] which assumes that the surface is homogeneous and without miscut or step bunching. For comparison with previous work, we repeat the traditional analysis here on data from our Ag(110) sample. Further justification for this pursuit is to shed light on the question of the interplay between roughening and miscut, a question dealt with by Nijs and co-workers.[25]

By performing the analysis near $l=0$, the difference between steps due to roughening and due to miscut becomes invisible. Moreover, as more and more steps are activated at higher temperatures, the effect of miscut and bunching of steps in the low-temperature phase becomes less important, so the traditional analysis becomes more and more justified. A more complete understanding of the relation between roughening and miscut would require an analysis of the data at values of l different from zero to ensure that the miscut is visible in the line shapes. We note, however, that such a procedure is difficult because the multiple-component profile shapes cannot be explained with a single power law (as in the theory[1] predicted). If the miscut is not respected, the fitted values of η would be meaningless and show the wrong l dependence.[14]

For the power-law line-shape analysis we used the theoretical profile shape predicted by the (anisotropic) BCSOS model valid for fcc(110) surfaces. This line shape, close to T_R reads[20] (with σ_x and σ_y the surface tensions)

$$I(h,k,l) \propto \left[\frac{1}{\sin^2(\pi l)}\right]\left[\left[\frac{\sigma_x}{\sigma_y}\right]^{1/2}(2\pi h)^2 + \left[\frac{\sigma_y}{\sigma_x}\right]^{1/2}(2\pi k)^2\right]^{(\eta-2)/2}, \tag{12a}$$

with

$$(\sigma_x(T_R)\sigma_y(T_R))^{1/2} = \frac{\pi}{2}k_B T_R \ . \tag{12b}$$

For fcc(110) surfaces, it is further expected that (note the adjustment to the surface coordinate frame and the *AB* stacking sequence of these surfaces)

$$\eta_{00}(l) = \frac{\pi k_B T}{4(\sigma_x\sigma_y)^{1/2}}[1-\cos(\pi l)] \ , \qquad \eta_{10}(l) = \eta_{01}(l) = \eta_{00}(1-l) \ . \tag{13}$$

As shown in the Appendix, the convolution of Eq. (12) with an ideal slit detector function can be approximated by a one-dimensional Lorentz-power-law (LPL) profile. We have therefore used LPL fits to the experimental diffraction profiles. These LPL profiles are of the functional form

$$I(h,l) \propto \frac{1}{\sin^2(\pi l)}\left[1+\frac{(2\pi h)^2}{\Gamma_x^2}\right]^{(\eta-2)/2}, \qquad I(k,l) \propto \frac{1}{\sin^2(\pi l)}\left[1+\frac{(2\pi k)^2}{\Gamma_y^2}\right]^{(\eta-2)/2} \tag{14}$$

with $\Gamma_x/\Gamma_y = \sigma_y/\sigma_x$. It must be noted that the use of formula (12) is only allowed for symmetrical surfaces and at temperatures T close to T_R. At low temperatures, deviations from Eq. (12) are possible, especially if there is a preferred step direction or a step bunching as shown in Sec. III A. These deviations are responsible for the profile shapes along $[\bar{1}10]$ exhibiting shoulders and an asymmetry, and make an analysis of the low-temperature $\eta(l)$ behavior impossible. This fact has already been noted in Ref. 14.

The out-of-phase profiles at $l=0$, however, are symmetrical and fairly well described by one single component along both azimuths. This makes an analysis of Eq. (12) at $l=0$ for both azimuths applicable. We note that this holds true although the miscut makes it impossible to extract the $\eta(l)$ behavior at other l values by use of Eq. (12). In the symmetrical power-law description, the profile tails, through η, act as a measure of surface roughness.

For details of the power-law profile fitting theory we refer to the literature.[1-14]

Two kinds of fit procedures have been employed. In the first the reflection profiles were fitted by convolving a Gaussian resolution function, $G(q)$, with a Lorentzian power-law function, $L_{\mathrm{PL}}(q)$. In order to account for the central peak, the Gaussian resolution function (0.002 reciprocal-lattice units FWHM) was added for $T<T_R$:

$$I(q)=cG(q)+G(q)\otimes L_{\mathrm{PL}}(q)\ , \tag{15}$$

where $\otimes$ denotes the convolution. The L_{PL} function is defined as

$$L_{\mathrm{PL}}(q)=\left[1+\frac{(q-q_0)^2}{\Gamma^2}\right]^{(\eta-2)/2} . \tag{16}$$

The respective amplitudes of the Gaussian and the Lorentz power-law function are fit parameters. The parameter q_0 defines the center of the reflection and Γ the width of L_{PL}. The power-law exponent η is a direct measure of the rate of logarithmic divergence and therefore of the surface roughness.

In a second and more simplified approach, we used the function

$$I(q)=cG(q)+L_{\mathrm{PL}}(q) \tag{17}$$

neglecting the convolution with the resolution function $G(q)$. We refer to this formalism as the pseudo-Voigt (PV) function.

The fits performed along both azimuths lead to comparable results. In Fig. 7 representative profiles of the (01) rod (scans along [001]) at $l=0.1$ are shown for temperatures between $T=420$ and 850 K. The experimental reflection profiles could be fitted with high accuracy, and the (normalized) goodness of the fit parameter, χ^2, was in all cases below 3, in most cases in the regime below 1.5 ($R_u\approx 2-5\,\%$).

The power-law exponent η and the constant c in Eqs. (15) and (17) are plotted as functions of the sample temperature in Fig. 8. The filled symbols represent results derived on the basis of the PV function, and the open symbols correspond to fits using the full convolution procedure. Both the fits along the [001] and [$\bar{1}$10] azimuths as well as the different fitting procedures used to describe the experimental profiles lead to similar results for η within an error of about ± 0.15. This indicates that despite the miscut the roughening theory is at $l=0$ (out-of-phase condition) indeed applicable (a nontrivial consequence), and further shows that the influence of details of the instrumental resolution function on the reflection profile *tails* is only small. The use of the Gaussian function to take account of the resolution function appears justified in view of the high quality of the fits. We note that the η values obtained, although fitted independently along [$\bar{1}$10] and [001], are within the error bars identical along both azimuths.

While the Bragg peak contribution c falls off rapidly with temperature (reaching 0 at about 850–900 K), the power-law exponent η is fairly constant (along both azimuths) between about 300 and 600 K, but then increases sharply [and roughly linearly, as predicted by Eq. (12)] above about 600 K. At 900 ± 20 K $\eta=1$ holds, as predicted by the surface roughening theory (Fig. 8). The value $T_R=900\pm 20$ K obtained from Fig. 8 is identical with the value obtained from the domain-matrix method (Sec. III A).

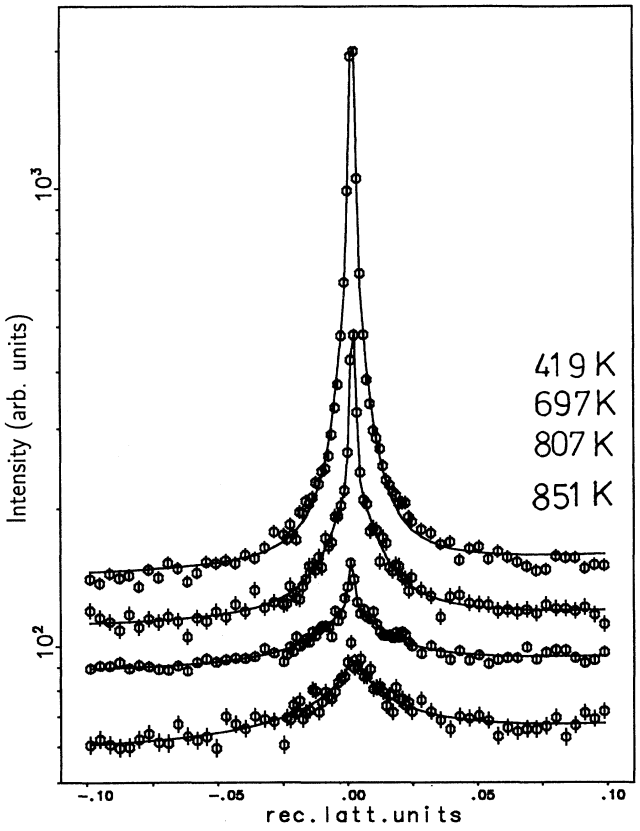

FIG. 7. Experimental profiles along [001] [transversal scan through the (0,1) rod] at $l=0.1$ (close to the out-of-phase condition $l=0$) where the profiles are symmetric. The LPL fits (solid lines) on the basis of Eqs. (15)–(17) fit well to the experimental data.

At low temperatures an initial roughness is present which can be related to the large terrace width fluctuations identified in Sec. III A. Details of the low-temperature surface morphology are, however, not extractable from the LPL fits at $l=0$, especially because the corresponding analysis at other l values is missing.

In this connection, it is interesting to note that den Nijs and co-workers[25] used the so-called RSOS model to predict a statistical pairing of up-steps and down-steps [the DOF (disordered flat phase)] at temperatures above some preroughening temperature T_{PR}. The interplay between entropy and further-than-nearest-neighbor interactions along [001] should stabilize the DOF phase according to the RSOS model. The predicted step pairing is obviously related to the tendency of the fcc(110) surfaces to form a (1×2) reconstruction at low temperatures which is an ordered array of up- and down-steps every second row. In the DOF phase, however, the steps are positionally disordered. The DOF phase has been predicted for fcc(110) surfaces with a slightly positive reconstruction energy, as is the case for Ag(110),[21] that (1×2) recon-

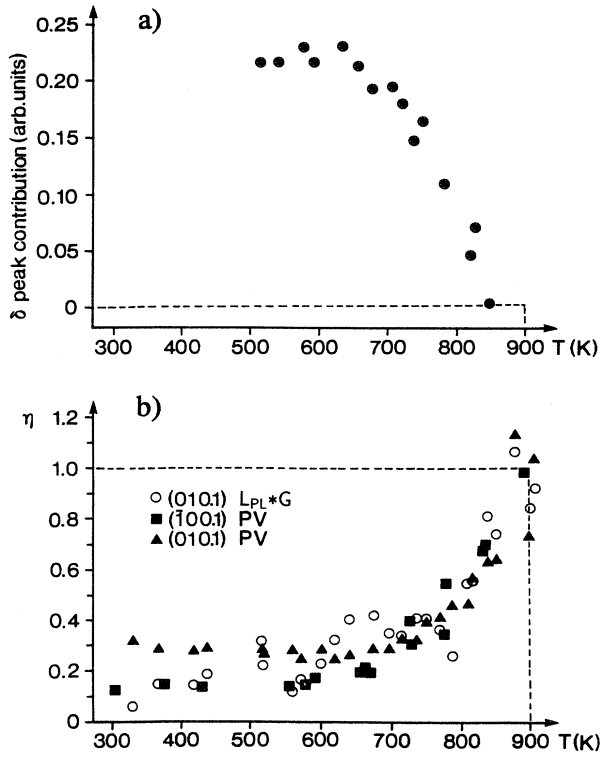

FIG. 8. Temperature evolution of (a) the δ peak contribution and (b) the roughening exponent η as determined from the out-of-phase profiles ($l=0.1$) along [$\bar{1}10$] and [001]. The data were derived on the basis of the pseudo-Voigt (PV) function (squares and triangles), and the L_{PL} function convolved with a Gaussian resolution function (circles), respectively. The roughening temperature is identified at 900±20 K, where $\eta=1$.

structs, e.g., upon K adsorption.[30]

A low preroughening temperature (<400 K) and therefore a high surface mobility already at room temperature would be consistent with the identified large terrace width fluctuations at low temperatures. It is, however, still open and not deducible from the diffraction profiles (mainly because of the meandering and bunching of the steps) whether a strict pairing of steps occurs along [001] (or would occur if no defects were present). The applicability of the RSOS theory may thus be prevented by either the defects (responsible for meandering and bunching) or the miscut or a combination of both.

In any case, however, the anisotropy of the BCSOS and the RSOS model is necessary to describe the low-temperature phase and the roughening behavior of Ag(110) which shows that the difference in the step energies along [$\bar{1}10$] and [001] is a relevant factor.

A second note concerns the change of the correlation function below and above the roughening temperature T_R. This change can now be interpreted in terms of the terrace widths and their size distribution. If the roughness is present at *all* length scales, it is a self-similar roughness. This self-similarity exists as long as a surface with random steps (with a microroughness) has regions of a macroscopic roughness as well. This is in general the case after the preparation process, i.e., a sputter and annealing cycle if total equilibrium is not yet reached. The surface is rough on macroscopic as well as microscopic scales. Above T_R, however, the surface is on a microscopic scale much more rough than it can be on a macroscopic one in order to be still a surface. Thus additional steps have been generated and the scale of the step distances has been reduced. The ratio of larger to smaller terraces, however, has changed in the opposite way: The larger terraces have grown at the expense of the smaller ones (not vice versa), although all terraces, of course, have become smaller. It is this compensation effect that makes the correlation function decrease *slower* in the rough phase (algebraical) than in the preroughe phase (exponentially), which is the realistic low-temperature phase for surfaces with low T_{PR}.

C. Determination of step energies J_x and J_y

The anisotropic BCSOS model now allows us to determine the step energies J_x and J_y, per atomic length unit, for steps running along $x=[\bar{1}10]$ and $y=[001]$. Theoretically, it holds that[20]

$$\frac{\Gamma_y}{\Gamma_x}=\frac{\sigma_x}{\sigma_y}=\frac{e^{-2J_x/k_BT}}{e^{-2J_y/k_BT}}\ ,\quad e^{-J_x/k_BT_R}+e^{-J_y/k_BT_R}=1\ . \tag{18}$$

The low-temperature asymmetry, together with T_R, therefore allows us to determine J_x and J_y, the coupling constants in the surface Hamiltonian:

$$H=\sum_{i,j}J_x[h_{i+1,j}-h_{i,j}]^2+J_y[h_{i,j+1}-h_{i,j}]^2\ , \tag{19}$$

which describes the (anisotropic) BCSOS (six-vertex model) model. h_{ij} here are height coordinates of the surface at the position (i,j) of the rectangular surface unit mesh (in the surface-adapted body-centered setting; see Ref. 22). For a mapping of the anisotropic BCSOS model to the six-vertex model, see Ref. 20.

The analysis of the step anisotropy on the Ag(110) surface (Sec. III A) now allows us to estimate the step energies under the assumption of equilibrium step structures. From the low-temperature (300 K) step density anisotropy of 3.5 (Sec. III A), analyzed at $l=0.5$, using $T_R=900\pm20$ K and Eq. (18), we obtain

$$\begin{aligned}J_x&=45\pm3\text{ meV}\ ,\\ J_y&=60\pm3\text{ MeV}\ ,\end{aligned} \tag{20}$$

and, furthermore,

$$k_BT_R=1.49\sqrt{J_xJ_y}\ . \tag{21}$$

We note that the power-law analysis (Sec. III B), performed at $l=0.1$, gives a consistent value of $\Gamma_x/\Gamma_y\approx3$ at 300 K and therefore a similar result.

The value 1.49 in Eq. (21) agrees remarkably well with the value 1.48±0.01 obtained from a Monte Carlo simulation study[26] performed for fcc(110) surfaces, and clearly exceeds $\pi/4=1.27$, the value expected in the isotopic

limiting case ($J_x = J_y = J$ along any direction; see, e.g., Ref. 3). This, together with the successful determination of J_x and J_y, is a *a posteriori confirmation* of the strongly anisotropic nature of the Ag(110) surface roughening transition.

IV. SUMMARY

We have investigated the thermally induced roughening of the Ag(110) surface using the domain-matrix method and an analytical power-law line-shape description. The sample was misoriented from (110) by about 0.14°(±0.05°) along the [$\bar{1}$10] and by less than 0.1° along the [001] azimuth. Both approaches employed to analyze the data give consistent results for the roughening temperature. The DMM provides information about the terrace width distribution and can therefore be viewed as a direct microscopical description of the step arrangements. On the other hand, the power-law formalism is more fundamental because it relates to the height-height correlation function in the continuum approximation. The power-law function, however, is only applicable at higher temperatures (close to T_R), where the steps are mainly of entropic origin and only one homogeneous diffraction component is present. The Ag(110) surface is found to undergo a roughening transition at $T_R = 900 \pm 20$ K. The regime between $T = 300$ K and T_R can be characterized by strongly fluctuating terrace widths. Along [$\bar{1}$10] these are best described by a bimodal distribution of steps with both a broad Gaussian terrace width distribution function and some rougher surface parts.

The low-temperature anisotropy of the surface (ratio of the step densities at 300 K) is about 3.5:1 which means that the close-packed [$\bar{1}$10] steps have a lower-energy cost than the less closed-packed steps along [001].

We devolved the formerly proposed *hill-and-valley* structure, which would be stabilized by a cusp in the surface free energy, into a two-component step model with bunching and meandering of steps. This satisfactorily explains the profile shapes along both azimuths at low temperatures. The bunching could be caused by defects (e.g., oxygen) well below the Auger detection limit.

Despite the low-temperature inhomogeneity, however, the 0.14° misaligned surface exhibits practically the same roughening temperature as other fcc(110) surfaces, if scaled to the bulk melting point. We find $T_R = 0.73 T_m$ which is close to theoretical and experimental expectations for fcc(110) surfaces varying from $0.69 T_m$ up to $0.75 T_m$. The thermal roughening of the surface takes place by the growth of the rough regions at the expense of the more flat ones. The terrace widths of both components decrease with temperature, and additional steps are formed on the original flat parts of the surface. When the roughening transition sets in, the step-step distance has reduced to only a small number of lattice constants (about 2).

The resulting roughening behavior is consistent with the theoretical expectations of the (anisotropic) BCSOS model predicting an anisotropic type of surface roughening transition with different step energies along [$\bar{1}$10] and [001]. A determination of the step energies gives reasonable values of $J_x = 45 \pm 3$ meV and $J_y = 60 \pm 3$ meV per atomic length unit. This, as well as the relation $k_B T_R = 1.49 \sqrt{J_x J_y}$, establishes the anisotropic character of the roughening transition on this fcc(110)-type surface.

Our work has also shown that the traditional method of line-shape fitting for rough surfaces can still be useful when the effects of the miscut are present. The data measured near the anti-Bragg condition ($l = 0.1$ here) are symmetric about $q_\parallel = 0$ because the distortion due to miscut on one side of the line shape is compensated for by an equivalent one on the other side. This allows the data to be fit, but does lead to an enlarged value at low temperatures, reflecting the inherent step density due to the miscut. However, the distortion becomes unimportant for temperatures near T_R, where the excited steps outnumber the effect of the miscut.

ACKNOWLEDGMENTS

One of the authors (H.L.M.) would like to thank AT&T for providing access to the beamline X16A, and for its hospitality during his visit to Brookhaven. The support of this work by the Bundesministerium für Forschung und Technologie under Grant No. 055WMIBB8 is gratefully acknowledged. Partial support came from the U.S. Department of Energy under Program No. DEFG02-91ER45439. NSLS is supported by the U.S. Department of Energy under Contract No. DEAC012-76CH0016.

APPENDIX

The convolution of the function [Eq. (12) with $a = b = 1$]

$$I_0(q_x, q_y) = \left[\left[\frac{\Gamma_y}{\Gamma_x} \right]^{1/2} q_x^2 + \left[\frac{\Gamma_x}{\Gamma_y} \right]^{1/2} q_y^2 \right]^{-(1-\eta/2)}, \tag{A1}$$

with an anisotropic detector function (in reciprocal space)

$$F(q_x, q_y) = \delta(q_x) g(q_y) \tag{A2}$$

results, for the measurement along $x = [\bar{1}10]$ (and analogously along [001]), in

$$\begin{aligned} I(q_x, q_y) &= \int\int [(q_x - q_x')^2 \Gamma_y + (q_y - q_y')^2 \Gamma_x]^{(\eta-2)/2} \\ &\quad \times \delta(q_x') g(q_y') dq_x' dq_y' \\ &= \int [q_x^2]^{(\eta-2)/2} \left[1 + \frac{\Gamma_x}{\Gamma_y} \frac{(q_y^2 - q_y'^2)}{q_x^2} \right]^{(\eta-2)/2} \\ &\quad \times g(q_y') dq_y' . \end{aligned} \tag{A3}$$

For the x-profile tails that carry information about the surface roughness (along x) it holds that $q_x \gg q_y$ and also $q_x \gg (q_y - q_y')$. To first order it therefore follows that

$$I(q_x,0)\simeq[q_x^2]^{(\eta-2)/2}\int\left[1+\frac{\eta-2}{2}\frac{\Gamma_x}{\Gamma_y}\frac{(q_y')^2}{q_x^2}\right]g(q_y')dq_y'$$
$$=c_1[q_x^2]^{(\eta-2)/2}\left[1+\frac{\eta-2}{2}\frac{\Gamma_x}{\Gamma_y}\frac{c_2}{q_x^2}\right]$$
$$\simeq c_1[q_x^2]^{(\eta-2)/2}\left[1+\frac{\Gamma_x}{\Gamma_y}\frac{c_2}{q_x^2}\right]^{(\eta-2)/2}$$
$$=c_1\left[q_x^2+c_2\frac{\Gamma_x}{\Gamma_y}\right]^{(\eta-2)/2}, \quad \text{(A4)}$$

with some integration constants c_1 and c_2 that depend on the slit width. From the final result [with $c=c_2/(\Gamma_x\Gamma_y)$]

$$I(q_x,0)\propto\left[1+\frac{\Gamma_y}{\Gamma_x}\frac{q_x^2}{c_2}\right]^{(\eta-2)/2}=\left[1+\frac{q_x^2}{c\Gamma_x^2}\right]^{(\eta-2)/2},$$
$$I(0,q_y)\propto\left[1+\frac{\Gamma_x}{\Gamma_y}\frac{q_y^2}{c_2}\right]^{(\eta-2)/2}=\left[1+\frac{q_y^2}{c\Gamma_y^2}\right]^{(\eta-2)/2}, \quad \text{(A5)}$$

it follows that the ratio of the half-widths of the L_{PL} functions is indeed Γ_x/Γ_y [Eq. (14)].

[1]E. H. Conrad, Prog. Surf. Sci. **39**, 65 (1992).
[2]W. K. Burton and N. Cabrera, Discuss. Faraday Soc. **5**, 33 (1949).
[3]B. Salanon, F. Fabre, J. Lapujoulade, and W. Selke, Phys. Rev. B **38**, 7385 (1988).
[4]K. S. Liang, E. B. Sirota, K. L. D'Amico, G. J. Hughes, and S. K. Sinha, Phys. Rev. Lett. **59**, 2447 (1987).
[5]J. Wollschläger and H. Henzler, Phys. Rev. B **44**, 13 031 (1991).
[6]F. Fabre, D. Gorse, J. Lapujoulade, and B. Salanon, Europhys. Lett. **3**, 737 (1987).
[7]E. H. Conrad, L. R. Allen, D. L. Blanchard, and T. Engel, Surf. Sci. **187**, 265 (1987).
[8]I. K. Robinson, E. H. Conrad, and D. S. Reed, J. Phys. (Paris) **51**, 103 (1990).
[9]K. Kern, in *Phase Transitions in Surface Films,* edited by H. Taub, G. Torzo, H. Lauter, and S. C. Fain (Plenum, New York, in press).
[10]Y. Cao and E. H. Conrad, Phys. Rev. Lett. **64**, 477 (1990).
[11]H.-N. Yang, T.-M. Lu, and G.-C. Wang, Phys. Rev. Lett. **63**, 1621 (1989); Phys. Rev. B **43**, 4714 (1991).
[12]J. C. Heyraud and J. J. Metois, J. Cryst. Growth **82**, 269 (1987).
[13]P. von Blanckenhagen, W. Schommers, and V. Voegel, J. Vac. Sci. Technol. A **5**, 649 (1987).
[14]I. K. Robinson, E. Vlieg, H. Hornis, and E. H. Conrad, Phys. Rev. Lett. **67**, 1890 (1991).
[15]G. A. Held, J. L. Jordan-Sweet, P. M. Horn, A. Mak, and R. J. Birgeneau, Phys. Rev. Lett. **59**, 2075 (1987).
[16]B. M. Ocko and S. G. J. Mochrie, Phys. Rev. B **38**, 7378 (1988).
[17]J. S. Ozcomert, W. W. Pai, N. C. Bartelt, and J. E. Reutt-Robey, Surf. Sci. **293**, 183 (1993); Phys. Rev. Lett. **72**, 258 (1994).
[18]G. A. Held, D. M. Goodstein, R. M. Feenstra, D. Y. Noh, and R. J. Birgenau, Phys. Rev. B **48**, 8458 (1993).
[19]S. Pflanz and W. Moritz, Acta. Crystallogr. Sect. A **48**, 716 (1992).
[20]H. van Beijeren and I. Nolden, in *Structures and Dynamics of Surfaces,* edited by W. Schommers and P. von Blanckenhagen (Springer, Heidelberg, 1987); H. van Beijeren, Phys. Rev. Lett. **38**, 993 (1973); R. W. Youngblood, J. D. Axe, and B. M. McCoy, Phys. Rev. B **21**, 5212 (1980); A. Trayanov, A. C. Levi, and E. Tosatti, Surf. Sci. **233**, 184 (1990); S. T. Chui, and J. D. Weeks, Phys. Rev. B **14**, 4978 (1976); J. M. Kosterlitz and D. J. Thouless, J. Phys. C **6**, 1181 (1973); J. M. Kosterlitz, *ibid.* **7**, 1046 (1974).
[21]P. H. Fuoss and I. K. Robinson, Nucl. Instrum. Methods Phys. Res. Sect. A **222**, 171 (1984); E. Vlieg, J. F. van der Veen, J. E. Macdonald, and M. Miller, J. Appl. Crystallogr. **20**, 330 (1987).
[22]The rectangular surface unit cell is related to the cubic setting by the following relations between the axes: $[100]_r=[001]$, $[010]_r=\frac{1}{2}[\bar{1}10]$, and $[001]_R=\frac{1}{2}[110]$.
[23]G. Wulff, Z. Kristallogr. Kristallgeom. Krystallphys. Kristallchem. **34**, 449 (1901); C. Herring, Phys. Rev. **82**, 87 (1951).
[24]C. Rottman and M. Wortis, Phys. Rev. B **29**, 328 (1984).
[25]K. Rommelse and M. den Nijs, Phys. Rev. Lett. **59**, 2578 (1987); M. den Nijs and K. Rommelse, Phys. Rev. B **40**, 4709 (1989); M. den Nijs, Phys. Rev. Lett. **64**, 435 (1990).
[26]V. Pontikis and V. Rosato, Surf. Sci. **162**, 150 (1985); W. J. Shugard, J. D. Weeks, and G. H. Gilmer, Phys. Rev. Lett. **41**, 1399 (1978).
[27]R. Kariotis, Surf. Sci. **248**, 306 (1991).
[28]R. Kariotis and M. G. Lagally, Surf. Sci. **248**, 295 (1991).
[29]N. C. Bartelt, T. L. Einstein, and E. D. Williams, Surf. Sci. Lett. **240**, L591 (1990).
[30]C. L. Fu and K. M. Ho, Phys. Rev. Lett. **63**, 1617 (1989); M. Okada, H. Tochihara, and Y. Murata, Phys. Rev. B **43**, 1411 (1991); Surf. Sci. **245**, 380 (1991).